

# Synchrotron break frequencies of mildly-to-highly relativistic outflows observed off-axis

Gilad Sadeh<sup>\*</sup>

*Dept. of Particle Phys. & Astrophys., Weizmann Institute of Science, Rehovot 76100, Israel*

Accepted XXX. Received YYY; in original form ZZZ

## ABSTRACT

We consider the synchrotron spectrum produced by mildly-to-highly relativistic collisionless shocks. Simple analytic formulae are derived for the break frequencies (peak frequency, self-absorption frequency, synchrotron and inverse Compton cooling frequencies) of the emission produced by post-shock plasma elements propagating at an angle  $\theta_e$  relative to the observer's line of sight. These formulae reproduce well the results of earlier exact analytic calculations valid for ultra-relativistic shocks and also hold for  $\gamma < 10$  and for "off-axis" propagation (deviating from the ultra-relativistic results by approximately an order of magnitude). Our results will improve parameter estimation accuracy from future observations of synchrotron emission produced by collisionless shocks driven by the relativistic ejected material from compact objects mergers and jetted tidal disruption events. The improved accuracy for mildly relativistic velocities is essential since most events will be observed off-axis, with  $\gamma < 10$  outflows dominating the synchrotron emission (due to relativistic beaming). For GW170817, our results imply that (i) the Lorentz factor of the plasma emitting the observed radiation is bounded by  $2.6 < \gamma$  at  $t \sim 10$  days and by  $\gamma < 12$  at  $t > 16$  days, (ii) the interstellar medium (ISM) density,  $n$ , and the fraction of internal energy density held by magnetic fields,  $\epsilon_B$ , are bounded by  $n \cdot \epsilon_B \lesssim 3 \times 10^{-7} \text{cm}^{-3}$ . In future merger events in higher-density ISM, the peak and cooling frequencies may be identified in the radio and X-ray bands; consequently,  $\gamma, n \cdot \epsilon_B$  could be measured as opposed to the case of GW170817, where these frequencies are out of the observable range.

**Key words:** (transients:) neutron star mergers – (transients:) black hole-neutron star mergers – gravitational waves – radio continuum: transients – relativistic processes

## 1 INTRODUCTION

GW170817 provided a prolonged, rich, and unique set of thermal and non-thermal electromagnetic radiation observations. During the first  $\sim 10$  days, observations of the optical (UV-IR) electromagnetic counterpart of GW170817 indicate ejecta of  $\approx 0.05M_\odot$  expanding at  $\beta > 0.1$  and undergoing continuous heating by radioactive decays (Arcavi et al. 2017; Nicholl et al. 2017; Metzger 2017). These findings are consistent with the characteristics of Kilonova (KN) emission (Li & Paczyński 1998). The non-thermal emission observed between radio to X-ray is consistent with synchrotron emission from relativistic electrons in a power-law distribution ( $dn_e/d\gamma_e \propto \gamma_e^{-p}$ ), with a constant power index,  $p = 2.17$ , between 10 to 1000 days with no sign of spectral evolution (Hallinan et al. 2017; Troja et al. 2017; Lyman et al. 2018; Margutti et al. 2018; Troja et al. 2020; Makhathini et al. 2021; Balasubramanian et al. 2021, 2022). The spectrum follows  $F_\nu \propto \nu^{(1-p)/2}$  at all times, indicating that the radio emission surpasses both the peak frequency,  $\nu_m$ , and the self-absorption frequency,  $\nu_a$ , while the X-ray emission lie below the cooling frequency,  $\nu_c$ . Notably, it means that the frequencies  $\nu_m$  and  $\nu_a$  are below  $\sim 1\text{GHz}$  (Dobie et al. 2018; Balasubramanian et al. 2021, 2022), and  $h\nu_c$  is above  $\sim 10\text{keV}$  (Troja et al. 2020, 2022) between 10 to 1000 days. These bounds constrain the source veloc-

ity, the medium density, and the fraction of energy held by magnetic fields.

As mentioned in Linial & Sari (2019), relativistic electrons undergo energy loss through two distinct mechanisms: (i) synchrotron emission and (ii) up-scattering of photons by inverse-Compton processes. The latter process relies on the presence of low-energy photons. During the initial 10 days, the KN serves as such a photon source, necessitating consideration of inverse-Compton cooling.

A superluminal centroid motion was observed in radio, and together with the HST localization of the early thermal component, it provides 4 different center of light localizations between 8 days to 230 days (Mooley et al. 2018; Ghirlanda et al. 2019; Mooley et al. 2022), implying an off-axis synchrotron emission of a relativistic outflow. The presence of plasma expanding at  $\gamma > 10$  (which is assumed by structured jet models) cannot be directly inferred from observations, which may be accounted for by a  $\gamma \gtrsim 5$  outflow (Mooley et al. 2022). The synchrotron break frequencies for an ultra-relativistic spherical blast wave were derived by Granot & Sari (2002). Linial & Sari (2019) estimated the effect of synchrotron and inverse-Compton cooling in the case of GW170817 while considering on-axis emission. They concluded that 9 days post-merger, the Lorentz factor,  $\gamma$ , must exceed 2.1. GW170817 occurred in an elliptical, low-density galaxy, NGC 4993 (Abbott et al. 2017); future merger events may occur in non-elliptical galaxies, with much higher ISM densities,  $n \sim 1\text{cm}^{-3}$ . In such a case, the break frequencies are expected to be observed in

<sup>\*</sup> E-mail: gilad.sade@weizmann.ac.il

radio and X-ray bands. Thus, accurately describing the synchrotron break frequencies would provide stringent constraints over the outflow velocity, observing angle, ISM density, and fractions of energy held by relativistic electrons and magnetic fields in the shocked plasma. Naturally, most of the mergers will be observed off-axis, and consequently, the emission is expected to be dominated by  $\gamma < 10$  shocked plasma due to relativistic beaming.

Off-axis relativistic jets with an observed afterglow in which a gamma-ray burst is not detected are known as orphan afterglows (Granot et al. 2002). These events are among the promising electromagnetic counterparts to compact objects merger (Metzger & Berger 2012). Recently, such an afterglow was observed to have a Lorentz factor of  $\gamma < 10$  (Perley et al. 2024). Additionally, there are indications that tidal disruption events can also generate mildly-to-highly relativistic outflows (Burrows et al. 2011; Saxton et al. 2017; Alexander et al. 2020; Andreoni et al. 2022; Pasham et al. 2023; Rhodes et al. 2023). Providing simple analytic expressions for the break frequencies for these types of outflows is essential for accurately determining their properties.

We derive the synchrotron break frequencies for a uniform volume element of shocked plasma propagating at mildly to highly relativistic velocities, considering both on-axis and off-axis observers. In this description, we assume that the velocity direction of the shocked plasma is perpendicular to the shock front, or equivalently,  $v_{\perp} \gg v_{\parallel}$ , where  $v_{\perp}/v_{\parallel}$  is the lab frame shocked plasma velocity component perpendicular/parallel to the shock front. It applies to various relativistic astrophysical phenomena, including: on-axis emission from a relativistic jet, off-axis emission from a structured jet for as long as the structure propagates radially (Govreen-Segal & Nakar (2023) showed that a power-law jet structure with  $dE/d\theta \propto \theta^{\gamma-3}$ , keeps its initial shape for  $\gamma \geq 3$ , indicating that the evolution of each angular bin can be approximated by Blandford-McKee evolution (Blandford & McKee 1976) such that the lateral spreading is negligible), off-axis emission from a relativistic jet as the Lorentz factor reaches  $\gamma \sim 1/\theta_v$  (where  $\theta_v$  is the viewing angle) and for a shocked plasma driven by ejecta that propagates into the ISM, such that the shock propagation can be approximated by a section of a spherical outflow (Sadeh 2024). For the self-absorption frequency, a specific geometrical structure is assumed. We further consider a power-law energy distribution for electrons, given by  $dn_e/d\gamma_e \propto \gamma_e^{-p}$ . Here,  $\gamma_e$  represents the electron Lorentz factor within the plasma's rest frame, while  $p$  is within the range of  $2 \leq p \leq 2.5$ . Simultaneously, fractions  $\varepsilon_e$  and  $\varepsilon_B$  correspond to the post-shock internal energy density proportions attributed to non-thermal electrons and magnetic fields, respectively. This phenomenological description, capturing the post-shock plasma conditions, finds support across a diverse spectrum of observations and plasma calculations encompassing both relativistic and non-relativistic shocks (see Blandford & Eichler 1987; Keshet & Waxman 2005; Waxman 2006; Keshet 2006; Bykov & Treumann 2011; Sironi et al. 2013; Pohl et al. 2020; Ligorini et al. 2021; Kobzar et al. 2021).

The paper is organized as follows. In § 2, we derive the analytic expressions for the synchrotron break frequencies. We compare our results to accurate analytic calculations and earlier estimations in § 3. Finally, in § 4, we discuss the implications of our analysis to GW170817 synchrotron observations, and our conclusions are summarized in § 5.

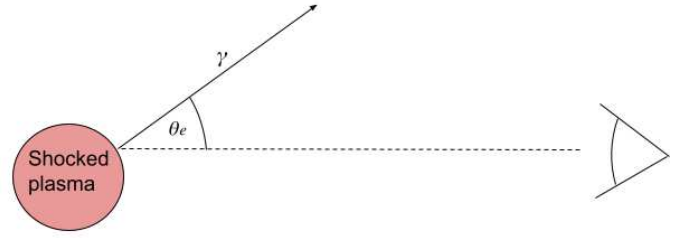


**Figure 1.** A schematic illustration of the conditions described in 2.

## 2 ANALYTIC EXPRESSIONS

We assume that the flux is primarily produced by a synchrotron-emitting blob consisting of uniformly shocked plasma with a Lorentz factor  $\gamma$ , moving through a homogeneous ISM with a number density  $n$ . Additionally, we assume that the dynamical evolution of the volume element is negligible while it remains the dominant source of the observed synchrotron emission. A spherical coordinate system is used, where the blob is located at a distance  $R$  from the origin. The observer is positioned such that the angle between the blob's velocity and the line of sight is  $\theta_e$  (see Fig. 1). We employ a phenomenological approach to describe synchrotron emission: the fraction of energy carried by electrons is denoted by  $\varepsilon_e$ , and the fraction of energy carried by magnetic fields is denoted by  $\varepsilon_B$ . We assume a power-law electron distribution within the shocked layers,  $dn_e/d\gamma_e \propto \gamma_e^{-p}$ . The characteristic plasma frame frequency of the synchrotron emission of electrons with Lorentz factor  $\gamma_e$  and isotropic velocity distribution is (Rybicki & Lightman 1979)

$$\nu_s \approx \frac{1}{3} \cdot \frac{3}{4\pi} \langle \sin \alpha \rangle \gamma_e^2 \frac{q_e B}{m_e c} \approx \gamma_e^2 \frac{q_e \sqrt{u_B}}{3m_e c}, \quad (1)$$

where the  $1/3$  factor is due to considering the peak emission in the spectrum and  $u_B$  is the (plasma frame) magnetic field energy density. Approximating the post shock energy density,  $2nm_p v^2$  (where  $v$  is the plasma velocity) for non-relativistic and  $4\gamma^2 nm_p c^2$  for highly relativistic shocks, by  $4\gamma(\gamma - 1)nm_p c^2$ , we have  $u_B = 4\varepsilon_B \gamma(\gamma - 1)nm_p c^2$ .

$$\nu_s = 0.7 \gamma_e^2 \frac{q_e \sqrt{\gamma(\gamma - 1) \varepsilon_B n m_p}}{m_e}. \quad (2)$$

In the lab frame, we have<sup>1</sup>

$$\nu = \frac{\nu_s}{\gamma(1 - \beta \cos(\theta_e))} = 0.7 \gamma_e^2 \sqrt{\frac{\gamma - 1}{\gamma}} \cdot \frac{q_e \sqrt{\varepsilon_B n m_p}}{m_e (1 - \beta \cos(\theta_e))}. \quad (3)$$

In this estimation, we assume the emitting region is relatively uniform and that the shocked material right behind the shock is dominating the synchrotron emission; these assumptions were validated for ultra-relativistic flows (Waxman 1997a,b; Granot & Sari 2002) and mildly-relativistic flows (Sadeh et al. 2023, 2024; Sadeh 2024). In realistic scenarios, there are various contributions to the flux from different angles and shocked plasma velocities. However, three points should be noted here: first, if the break frequencies are not observed, as in the case of GW170817, the bounds provided by this analysis would be consistent with all of the various optional  $\theta_e$  and  $\gamma$ . Second, if indeed there are competing contributions from two separate regions of considerably different  $\theta_e$  and  $\gamma$ , the break frequencies would be

<sup>1</sup> The first order corrections in  $v_{\parallel}/v_{\perp}$  are  $\theta_e \rightarrow \theta_e \pm \frac{v_{\parallel}}{v_{\perp}}$ ,  $\beta \rightarrow \beta$ ,  $\gamma \rightarrow \gamma$ .

significantly smeared, and this analysis can be used to reconstruct such a smear in the spectrum. Third, in case the break frequencies are observed with distinct values, it is reasonable to assume most of the contribution arrives from tightly distributed values of  $\theta_e$  and  $\gamma$ .

## 2.1 Peak frequency

For a power-law distribution of electrons  $dn_e/d\gamma_e \propto \gamma_e^{-p}$  (between  $\gamma_{\min}$  and  $\gamma_{\max}$ )  $\gamma_{\min}$  is obtained by requiring the average energy per electron to equal a fraction  $\varepsilon_e$  of the post-shock internal energy per particle,  $(\gamma - 1)m_p c^2$ . the minimal energy electrons Lorentz factor is (Sadeh et al. 2023)

$$\gamma_{\min} = \frac{l_p(\gamma - 1) \varepsilon_e m_p}{p - 1} \frac{1}{m_e}, \quad (4)$$

where

$$l_p = \frac{p - 2}{1 - (\gamma_{\max}/\gamma_{\min})^{2-p}}, \quad l_p \xrightarrow{p \rightarrow 2} \frac{1}{\ln(\gamma_{\max}/\gamma_{\min})}. \quad (5)$$

The observed frequency from these electrons is (from Eq. (3))

$$\nu_m = 0.7 \left( \frac{l_p(\gamma - 1) \varepsilon_e m_p}{p - 1} \frac{1}{m_e} \right)^2 \sqrt{\frac{\gamma - 1}{\gamma}} \cdot \frac{q_e \sqrt{\varepsilon_B n m_p}}{m_e (1 - \beta \cos(\theta_e))}. \quad (6)$$

For  $p = 2.17$

$$\nu_m = 1.5 \varepsilon_{e,-1}^2 \varepsilon_{B,-2}^{\frac{1}{2}} n_{-3}^{\frac{1}{2}} \frac{\gamma^{-\frac{1}{2}} (\gamma - 1)^{\frac{5}{2}}}{(1 - \beta \cos(\theta_e))} \text{MHz}, \quad (7)$$

where the prefactor varies up to a factor of  $\sim 4$  for  $2 < p < 2.5$ .

## 2.2 Self-absorption frequency

Following Sadeh et al. (2024) we estimate the self-absorption frequency at time  $t$  as the frequency for which  $\tau_\nu = \alpha_\nu \Delta_\tau = 1$ , where  $\alpha_\nu$  and  $\Delta_\tau$  are the typical absorption coefficient and the typical path length traversed by photons through the shocked plasma, when the forward shock reached the radius  $R$ , dominating the emission of radiation observed at time  $t$ . In this analysis, we approximate the geometry of the shocked plasma as a narrow conical section of a spherical blast wave with an angle  $\theta_e$  between the cone symmetry axis and the line of sight. We estimate the thickness  $\Delta_R$  of the emitting layer by conservation of particle number as

$$\Delta_R \approx \frac{R}{12\gamma^2}, \quad (8)$$

and

$$\Delta_\tau \approx \frac{\Delta_R}{\cos \theta_e} \approx \frac{\beta c t}{(12\gamma^2 \cos(\theta_e))(1 - \beta \cos(\theta_e))}. \quad (9)$$

To derive the self-absorption frequency in the observer frame (primed,  $'$ , quantities are in the shocked plasma frame), we first approximate the absorption coefficient, which is given by (Rybicki & Lightman 1979)

$$\alpha_\nu = \frac{\nu'}{v} \alpha'_\nu \approx \gamma^{\frac{2-p}{4}} (1 - \beta \cos(\theta_e))^{-\frac{p+2}{2}} (\gamma - 1)^{\frac{5p-2}{4}} f_a(p) \nu^{-\frac{p+4}{2}}, \quad (10)$$

where

$$f_a(p) = (p - 1) \left( \frac{p - 2}{p - 1} \frac{\varepsilon_e m_p}{1 - (\gamma_{\max}/\gamma_{\min})^{2-p}} \right)^{p-1} 4n \left( \frac{2\pi m_e c}{3q_e} \right)^{-\frac{p}{2}} \times \frac{(32\pi \varepsilon_B n m_p c^2)^{\frac{p+2}{4}} \sqrt{3} q_e^3 \sqrt{\pi} \Gamma\left(\frac{p+6}{4}\right)}{8\pi m_e^2 c^2} \frac{1}{2} \frac{\Gamma\left(\frac{p+6}{4}\right)}{\Gamma\left(\frac{p+8}{4}\right)} \Gamma\left(\frac{3p+22}{12}\right) \Gamma\left(\frac{3p+2}{12}\right).$$

(11)

The optical depth at (observed) frequency  $\nu$  is given by

$$\tau_\nu \approx \alpha_\nu \Delta_\tau \approx \frac{\beta c t \gamma^{\frac{2-p}{4}} (1 - \beta \cos(\theta_e))^{-\frac{p+2}{2}} (\gamma - 1)^{\frac{5p-2}{4}} f_a(p) \nu^{-\frac{p+4}{2}}}{(12\gamma^2 \cos(\theta_e))(1 - \beta \cos(\theta_e))}. \quad (12)$$

The self-absorption frequency,  $\nu_a$  defined by  $\tau_\nu(\nu = \nu_a) = 1$ , is finally given by

$$\nu_a = \left( \frac{\beta c t \gamma^{\frac{2-p}{4}} (\gamma - 1)^{\frac{5p-2}{4}} f_a(p)}{12\gamma^2 \cos(\theta_e)(1 - \beta \cos(\theta_e))^{\frac{p+4}{2}}} \right)^{\frac{2}{p+4}}. \quad (13)$$

## 2.3 Synchrotron Cooling frequency

$\gamma_c^{\text{syn}}$  is obtained by requiring the (plasma frame) synchrotron loss time (Sadeh et al. 2024),  $m_e c^2 / (\gamma_e (4/3) \sigma_T c u_B)$ , to be equal to the time measured at the plasma frame,  $t/\gamma/(1 - \beta \cos(\theta_e))$ .

$$\gamma_c^{\text{syn}} = \frac{(1 - \beta \cos(\theta_e)) m_e}{4(\gamma - 1) \varepsilon_B \left(\frac{4}{3}\right) \sigma_T n m_p c t}. \quad (14)$$

Notice that this derivation assumes that  $\int \beta dt \approx \beta \cdot t$ , an order unity factor is ignored and the formula has to be tested for the specific cases we consider. It is shown to be accurate for a case of shocked plasma driven by ejecta propagating radially in Sadeh et al. (2024) and for an ultra-relativistic blast wave propagating radially in § 3. The observed frequency from these electrons is

$$h\nu_c^{\text{syn}} = 0.7 \left( \frac{(1 - \beta \cos(\theta_e)) m_e}{4(\gamma - 1) \varepsilon_B \left(\frac{4}{3}\right) \sigma_T n m_p c t} \right)^2 \sqrt{\frac{\gamma - 1}{\gamma}} \cdot \frac{h q_e \sqrt{\varepsilon_B n m_p}}{m_e (1 - \beta \cos(\theta_e))}. \quad (15)$$

Which can be written as

$$h\nu_c^{\text{syn}} = 9.1 t_{155}^{-2} \varepsilon_{B,-2}^{-\frac{3}{2}} n_{-3}^{-\frac{3}{2}} \frac{1 - \beta \cos(\theta_e)}{\gamma^{\frac{1}{2}} (\gamma - 1)^{\frac{3}{2}}} \text{keV}, \quad (16)$$

where  $t_{155} = t/155 \text{days}$ .

## 2.4 Inverse Compton cooling

$\gamma_c^{\text{IC}}$  is obtained by requiring the (plasma frame) inverse-Compton loss time,  $m_e c^2 / (\gamma_e (4/3) \sigma_T c u_\gamma)$ , to be equal to the time measured at the plasma frame,  $t/\gamma/(1 - \beta \cos(\theta_e))$ .

$$\gamma_c^{\text{IC}} = \frac{\gamma (1 - \beta \cos(\theta_e)) m_e c}{u_\gamma \left(\frac{4}{3}\right) \sigma_T t} = \frac{\gamma^3 \beta^2 3\pi m_e c^4 t}{\sigma_T L_{\text{bol}} (1 - \beta \cos(\theta_e))}, \quad (17)$$

where the photon energy density,  $u_\gamma$ , is given by (Linial & Sari 2019)

$$u_\gamma = \frac{L_{\text{bol}}}{4\pi R^2 c} \cdot \frac{1}{\gamma^2} = u_\gamma = \frac{L_{\text{bol}}}{4\pi c^3 t^2} \cdot \frac{(1 - \beta \cos(\theta_e))^2}{\gamma^2 \beta^2}. \quad (18)$$

The observed frequency from these electrons is

$$h\nu_c^{\text{IC}} = 0.7 \left( \frac{\gamma^3 \beta^2 3\pi m_e c^4 t}{\sigma_T L_{\text{bol}} (1 - \beta \cos(\theta_e))} \right)^2 \sqrt{\frac{\gamma - 1}{\gamma}} \cdot \frac{h q_e \sqrt{\varepsilon_B n m_p}}{m_e (1 - \beta \cos(\theta_e))}. \quad (19)$$

Which can be written as

$$h\nu_c^{\text{IC}} = 5.1 L_{\text{bol},40}^{-2} t_{10}^2 \varepsilon_{B,-2}^{\frac{1}{2}} n_{-3}^{\frac{1}{2}} \frac{\gamma^{\frac{11}{2}} \beta^4 (\gamma - 1)^{\frac{1}{2}}}{(1 - \beta \cos(\theta_e))^3} \text{eV}, \quad (20)$$

where  $L_{\text{bol},40} = L_{\text{bol}}/10^{40} \text{erg/s}$ .

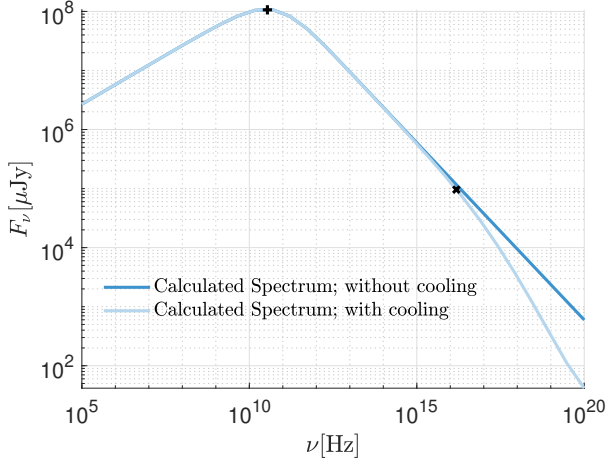


**Figure 2.** Calculated synchrotron spectrum following [Gruzinov & Waxman \(1999\)](#) for the following parameters  $\{E, n, t, \varepsilon_e, \varepsilon_B, p\} = \{10^{55}\text{erg}, 1\text{cm}^{-3}, 2\text{days}, 5 \times 10^{-2}, 10^{-4}, 2.2\}$  with and without synchrotron cooling. The analytic  $\nu_m$  and  $\nu_c$ , Eqs. (7) and (16), are shown by '+' and 'x' signs respectively.

### 3 COMPARISON TO EARLIER RESULTS

#### 3.1 Full calculation of spherical ultra-relativistic blast wave

In [Gruzinov & Waxman \(1999\)](#), an accurate analytic calculation is provided for the synchrotron light curve and spectrum of a spherical ultra-relativistic strong explosion ([Blandford & McKee 1976](#)). In Fig. 2, we provide the full accurate spectrum calculated for a given set of parameters  $\{E, n, t, \varepsilon_e, \varepsilon_B, p\} = \{10^{55}\text{erg}, 1\text{cm}^{-3}, 2\text{days}, 5 \times 10^{-2}, 10^{-4}, 2.2\}$ , following [Gruzinov & Waxman \(1999\)](#) with and without synchrotron cooling. The proper relation between the observed time and the shocked plasma Lorentz factor, in this case, is  $t \approx R/4\gamma^2c$ , where  $R$  is the shock radius ([Sari et al. 1998; Sari 1998](#)). Since the explosion is ultra-relativistic,  $\gamma \gg 1$ , we use  $\cos \theta_e \approx 1$ . Thus the relation between the emitting plasma Lorentz factor and the observed time is ([Blandford & McKee 1976](#))

$$\gamma = \left( \frac{17}{1024\pi} \cdot \frac{E}{nm_p c^5} \cdot \frac{1}{t^3} \right)^{\frac{1}{8}}, \quad (21)$$

where we assumed here that most of the emission arrives from the shocked plasma right behind the shock. Our analytic estimations for  $\nu_m$  and  $\nu_c$  are added to Fig. 2 with good agreement.

#### 3.2 Previous analytical estimations

In [Granot & Sari \(2002\)](#), analytic estimation for  $\nu_m$  was presented for the case of a spherical ultra-relativistic strong explosion ([Blandford & McKee 1976](#)) that is later used in the context of GW170817 by [Gill et al. \(2019\)](#). In Fig. 3, we show the ratio between this estimation to our extension from Eq. (7) using Eq. (21) for various Lorentz factors and off-axis observers.

In [Linial & Sari \(2019\)](#), analytic estimations for both  $\nu_c^{\text{syn}}$  and  $\nu_c^{\text{IC}}$  are presented for the case of ultra-relativistic outflow emitting on-axis, later used in the context of GW170817. In Figs. 4–5, we show the ratio between those estimations to our extensions in Eqs. (16) and (20) for various Lorentz factors and off-axis observers.

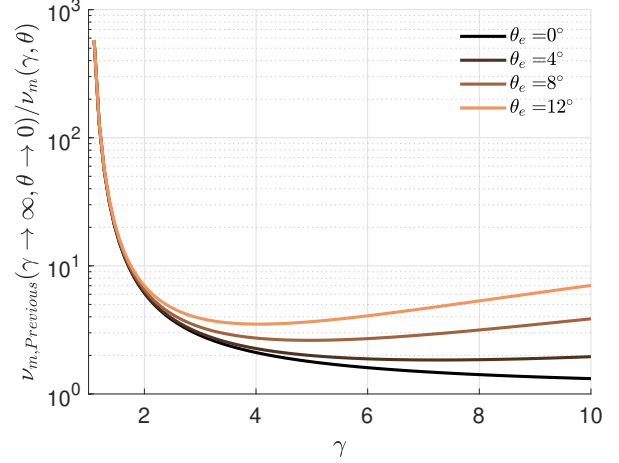


**Figure 3.** The ratio between the analytical estimation from [Granot & Sari \(2002\)](#) for  $\nu_m$ , which is valid in the limit of  $\theta = 0, \gamma \rightarrow \infty$ , to our extension given in Eq. (7) for various Lorentz factors and viewing angles. We use Eq. (21) to adjust to the spherical ultra-relativistic strong explosion.

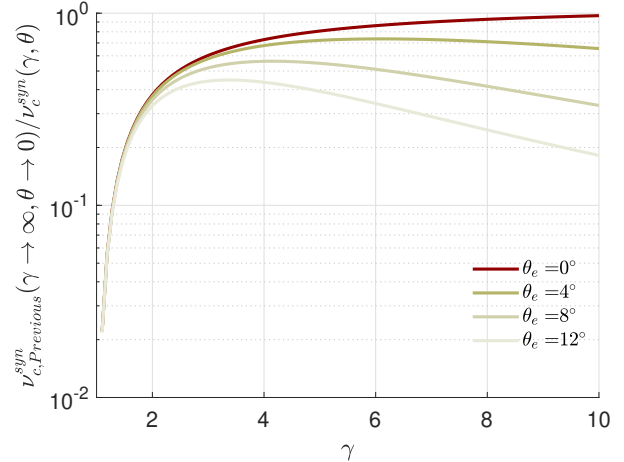


**Figure 4.** The ratio between the analytical estimation from [Linial & Sari \(2019\)](#) for  $\nu_c^{\text{syn}}$ , which is valid in the limit of  $\theta = 0, \gamma \rightarrow \infty$ , to our extension given in Eq. (16) for various Lorentz factors and viewing angles.

### 4 GW170817 IMPLICATIONS

The ratio to X-ray observations of GW170817 between 10 – 1000 days are consistent with a spectrum of  $F_\nu \propto \nu^{(1-p)/2}$ , with  $p = 2.17$ , implying  $\nu_m, \nu_a < 2.5\text{GHz}$  ([Dobie et al. 2018; Balasubramanian et al. 2021, 2022](#)) and  $h\nu_c^{\text{syn}}, h\nu_c^{\text{IC}} > 10\text{keV}$  ([Troja et al. 2020, 2022](#)). The observed superluminal centroid motion between 70 to 230 days indicates  $\theta_e > 5^\circ$  and  $\gamma \geq 4$  ([Mooley et al. 2018, 2022](#)). Emission from shocked plasma with Lorentz factor  $\gamma$  would be dominant only for angles  $\theta_e < \sin^{-1}(\frac{1}{\gamma})$  due to relativistic beaming. Considering all of the above, we provide bounds for the shocked plasma parameter space. There is no constraint from  $\nu_a$  due to the low ISM density.

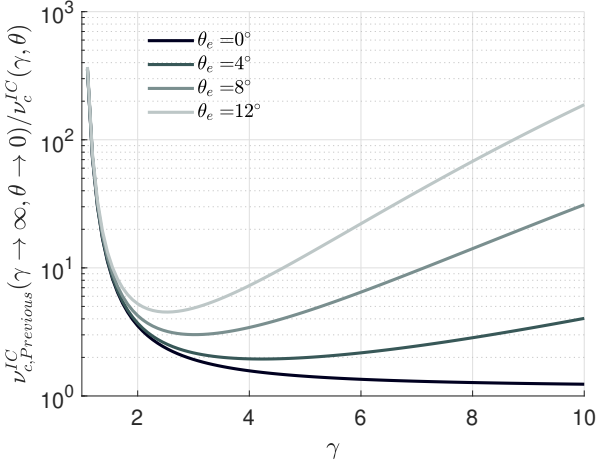


**Figure 5.** The ratio between the analytical estimation from Linial & Sari (2019) for  $\nu_c^{IC}$ , which is valid in the limit of  $\theta = 0$ ,  $\gamma \rightarrow \infty$ , to our extension given in Eq. 20 for various Lorentz factors and viewing angles.

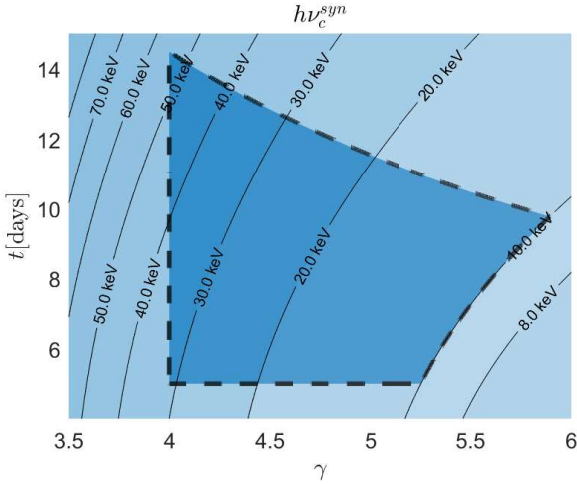


**Figure 6.** In dark blue: The allowed parameter space for  $h\nu_c^{syn} > 10\text{keV}$ ,  $\theta_e > 5^\circ$ ,  $\gamma \geq 4$ , and  $\theta_e < \sin^{-1}\left(\frac{1}{\gamma}\right)$ . The black lines represent equal  $h\nu_c^{syn}$  curves. we used  $\varepsilon_{B,-2n-3} = 0.01$ ,  $3.5 < \gamma < 6$ , and  $t_{155} = 1$

## 4.1 Synchrotron break frequencies constraints

### 4.1.1 $\nu_c^{syn}$

From Eq. 16 we find

$$9.1 t_{155}^{-2} \varepsilon_{B,-2n-3}^{-\frac{3}{2}} \frac{1 - \beta \cos(\theta_e)}{\gamma^{\frac{3}{2}} (\gamma - 1)^{\frac{3}{2}}} > 10. \quad (22)$$

At 155 days (the peak time), we have

$$\varepsilon_{B,-2n-3}^{-\frac{3}{2}} t_{155}^{-2} \frac{1 - \beta \cos(\theta_e)}{\gamma^{\frac{3}{2}} (\gamma - 1)^{\frac{3}{2}}} > 1.1. \quad (23)$$

Considering the abovementioned bounds, Eq. 23 has a solution only for  $\varepsilon_{B,-2n-3} \leq 0.03$ . In Fig. 6 we show an example for the possible parameter space for  $\varepsilon_{B,-2n-3} = 0.01$ ,  $3.5 < \gamma < 6$ ,  $t_{155} = 1$  and  $4^\circ < \theta_e < 15^\circ$ .

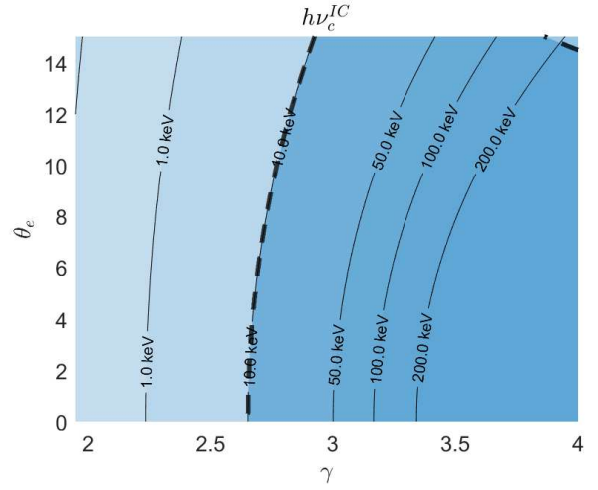


**Figure 7.** In dark blue: The allowed parameter space for  $h\nu_c^{IC} > 10\text{keV}$ . The black lines represent equal  $h\nu_c^{IC}$  curves. We used  $\varepsilon_{B,-2n-3} = 0.03$  and  $t = 9$ .

### 4.1.2 $\nu_c^{IC}$

From Eq. 20 we find

$$5.1 L_{\text{bol},40}^{-2} t_{10}^2 \varepsilon_{B,-2n-3}^{\frac{1}{2}} \frac{\gamma^{\frac{11}{2}} \beta^4 (\gamma - 1)^{\frac{1}{2}}}{(1 - \beta \cos(\theta_e))^3} > 10000. \quad (24)$$

Since we know that at 9days The bolometric luminosity from the KN is  $L_{\text{bol}} = 6 \times 10^{40}$  (Linial & Sari 2019) we can write

$$\varepsilon_{B,-2n-3}^{\frac{1}{2}} \frac{\gamma^{\frac{11}{2}} \beta^4 (\gamma - 1)^{\frac{1}{2}}}{(1 - \beta \cos(\theta_e))^3} > 87757, \quad (25)$$

In Fig. 7 we show the possible parameter space for  $\varepsilon_{B,-2n-3} = 0.03$ ,  $1 < \gamma < 10$ ,  $t = 9$  days and  $0^\circ < \theta_e < 10^\circ$ . We find a lower bound for the Lorentz factor of  $\gamma > 2.6$ .

### 4.1.3 $\nu_m$

The actual electron distribution in realistic conditions is not a pure power-law; the electrons are expected to be in a thermal population with a high energy power-law tail. As such, a proper bound for GW170817  $\nu_m$  would be  $\nu_m \ll 2.5\text{GHz}$ . Using a bound of  $\nu_m < 0.5\text{GHz}$  together with Eq. (7) we find

$$\varepsilon_{e,-1}^2 \varepsilon_{B,-2n-3}^{\frac{1}{2}} \frac{\gamma^{-\frac{1}{2}} (\gamma - 1)^{\frac{5}{2}}}{(1 - \beta \cos(\theta_e))} < 731. \quad (26)$$

In Fig. 8, we show the possible parameter space for  $p = 2.17$ ,  $\varepsilon_{e,-1}^2 \varepsilon_{B,-2n-3}^{\frac{1}{2}} = 0.07$ ,  $6 < \gamma < 12$  and  $0^\circ < \theta_e < 12^\circ$ . The values of  $\varepsilon_{e,-1}^2 \varepsilon_{B,-2n-3}^{\frac{1}{2}} = 0.07$  are considerably small so we find it reasonable to put an upper bound over Lorentz factor of  $\gamma < 12$  for the emitting shocked plasma for  $t > 16\text{days}$  (first radio observations).

## 4.2 Previous fits to GW170817

Some of the previous fits to the synchrotron observations of GW170817 provide values in tension with the abovementioned bounds. For example, in many semi-analytical calculations, the best fits found indicate  $\varepsilon_{B,-2n-3} = 0.1 - 1$ , suggesting that it is essential that the bounds from the spectrum analysis should be incorporated

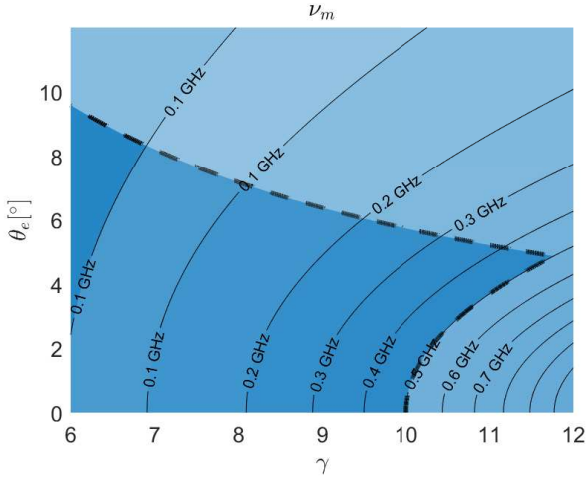


**Figure 8.** In dark blue: The allowed parameter space for  $\nu_m > 0.5\text{GHz}$ , and  $\theta_e < \sin^{-1}\left(\frac{1}{\gamma}\right)$ . The black lines represent equal  $\nu_m$  curves. We used  $p = 2.17$  and  $\varepsilon_{e,-1}^2 \varepsilon_{B,-2}^{\frac{1}{2}} n_{-3}^{\frac{1}{2}} = 0.07$ .

into the fitting pipeline. Furthermore, it is important to notice that the potential jet structure that fits the rising non-thermal light curve of GW170817 is consistent with the lower bounds over the shocked plasma Lorentz factor,  $\gamma > 2.6$ .

## 5 CONCLUSIONS

In this work, we derived analytical expressions for the synchrotron break frequencies, namely  $\nu_m$ ,  $\nu_a$ ,  $\nu_c^{\text{syn}}$  and  $\nu_c^{\text{IC}}$  from shocked plasma that are valid for both mildly-relativistic and ultra-relativistic outflows and for both on- and off-axis observers, extending the validity of previous analytic estimations which were valid for on-axis emission and ultra-relativistic velocities (see Figs. 3-5 in § 3). Our analytic formulae for  $\nu_m$  and  $\nu_c^{\text{syn}}$  were tested successfully for the fully accurate analytic solution in the case of an ultra-relativistic spherical blast wave (see Fig. 2). Our analytic formulae for  $\nu_c^{\text{IC}}$  is based on the same calculation as  $\nu_c^{\text{syn}}$ , and our analytic formula for  $\nu_a$  was successfully tested for specific cases of mildly relativistic ejecta in [Sadeh et al. \(2024\)](#).

These results will be useful for accurate parameter estimation ( $n$ ,  $\gamma$ ,  $\theta_e$ ,  $\varepsilon_B$ , and  $\varepsilon_e$ ) from future merger events and jetted TDEs since most of them will be observed off-axis, and the synchrotron emission is expected to be dominated by  $\gamma < 10$  shocked plasma due to the relativistic beaming. In typical ISM densities, ( $n \sim 1\text{cm}^{-3}$ ), the break frequencies are expected to be observed in radio and X-ray. Consequently, the analytic formulae derived in this paper would provide more significant constraints than those derived for GW170817.

Applying our derived analytic formulae for the case of GW170817 provided bounds over the ISM density,  $n$ , and the fraction of energy held by magnetic fields  $\varepsilon_B$  such that  $n \cdot \varepsilon_B \leq 3 \times 10^{-7}\text{cm}^{-3}$ . The Lorentz factor of the emitting shocked plasma is bounded by  $\gamma > 2.6$  at  $t \sim 10\text{days}$  and  $\gamma < 9.5$  at  $t < 230\text{days}$ . Some of the results trying to fit the synchrotron emission data of GW170817 are in tension with these bounds (see §4). For any robust attempt to fit future similar events, it's essential to take into account the synchrotron break frequencies. This consideration is crucial to ensure the model's validity, particularly in light of the non-trivial constraints discussed above.

## ACKNOWLEDGEMENTS

We thank Eli Waxman and Andrei Gruzinov for their helpful contribution and insightful comments.

## DATA AVAILABILITY

The data underlying this article will be shared following a reasonable request to the corresponding author.

## REFERENCES

- Abbott B. P., et al., 2017, *The Astrophysical Journal*, 848, L12
- Alexander K. D., van Velzen S., Horesh A., Zauderer B. A., 2020, *Space Science Reviews*, 216, 81
- Andreoni I., et al., 2022, *Nature*, 612, 430
- Arcavi I., et al., 2017, *Nature*, 551, 64
- Balasubramanian A., et al., 2021, *The Astrophysical Journal Letters*, 914, L20
- Balasubramanian A., et al., 2022, *The Astrophysical Journal*, 938, 12
- Blandford R., Eichler D., 1987, *Physics Reports*, 154, 1
- Blandford R. D., McKee C. F., 1976, *The Physics of Fluids*, 19, 1130
- Burrows D. N., et al., 2011, *Nature*, 476, 421
- Bykov A. M., Treumann R. A., 2011, *The Astronomy and Astrophysics Review*, 19, 42
- Dobie D., et al., 2018, *The Astrophysical Journal*, 858, L15
- Ghirlanda G., et al., 2019, *Science*, 363, 968
- Gill R., Granot J., Colle F. D., Urrutia G., 2019, *The Astrophysical Journal*, 883, 15
- Govreen-Segal T., Nakar E., 2023, The Structure and Evolution of Relativistic Jetted Blast Waves, doi:10.48550/arXiv.2311.09297, <https://ui.adsabs.harvard.edu/abs/2023arXiv231109297G>
- Granot J., Sari R., 2002, *The Astrophysical Journal*, 568, 820
- Granot J., Panaitescu A., Kumar P., Woosley S. E., 2002, *The Astrophysical Journal*, 570, L61
- Gruzinov A., Waxman E., 1999, *The Astrophysical Journal*, 511, 852
- Hallinan G., et al., 2017, *Science*, 358, 1579
- Keshet U., 2006, *Physical Review Letters*, 97, 221104
- Keshet U., Waxman E., 2005, *Physical Review Letters*, 94
- Kobzar O., Niemiec J., Amano T., Hoshino M., Matsukiyo S., Matsumoto Y., Pohl M., 2021, *The Astrophysical Journal*, 919, 97
- Li L.-X., Paczyński B., 1998, *The Astrophysical Journal*, 507, L59
- Ligorini A., et al., 2021, *Monthly Notices of the Royal Astronomical Society*, 502, 5065
- Linial I., Sari R., 2019, *Monthly Notices of the Royal Astronomical Society*, 483, 624
- Lyman J. D., et al., 2018, *Nature Astronomy*, 2, 751
- Makhathini S., et al., 2021, *The Astrophysical Journal*, 922, 154
- Margutti B., et al., 2018, *The Astrophysical Journal*, 856, L18
- Metzger B. D., 2017, Technical report, Welcome to the Multi-Messenger Era! Lessons from a Neutron Star Merger and the Landscape Ahead, <https://ui.adsabs.harvard.edu/abs/2017arXiv171005931M>, <https://ui.adsabs.harvard.edu/abs/2017arXiv171005931M>
- Metzger B. D., Berger E., 2012, *The Astrophysical Journal*, 746, 48
- Mooley K. P., et al., 2018, *Nature*, 561, 355
- Mooley K. P., Anderson J., Lu W., 2022, *Nature*, 610, 273
- Nicholl M., et al., 2017, *The Astrophysical Journal*, 848, L18
- Pasham D. R., et al., 2023, *Nature Astronomy*, 7, 88
- Perley D. A., et al., 2024, AT2019pim: A Luminous Orphan Afterglow from a Moderately Relativistic Outflow, doi:10.48550/arXiv.2401.16470, <https://ui.adsabs.harvard.edu/abs/2024arXiv240116470P>
- Pohl M., Hoshino M., Niemiec J., 2020, *Progress in Particle and Nuclear Physics*, 111, 103751
- Rhodes L., et al., 2023, *Monthly Notices of the Royal Astronomical Society*, 521, 389

- Rybicki G. B., Lightman A. P., 1979, Radiative processes in astrophysics. <https://ui.adsabs.harvard.edu/abs/1979rpa..book.....R>
- Sadeh G., 2024, Non-thermal emission from mildly relativistic tidal ejecta of compact objects merger, [doi:10.48550/arXiv.2406.01338](https://doi.org/10.48550/arXiv.2406.01338), <http://arxiv.org/abs/2406.01338>
- Sadeh G., Guttman O., Waxman E., 2023, *Monthly Notices of the Royal Astronomical Society*, 518, 2102
- Sadeh G., Linder N., Waxman E., 2024, *Monthly Notices of the Royal Astronomical Society*, 531, 3279
- Sari R., 1998, *The Astrophysical Journal*, 494, L49
- Sari R., Piran T., Narayan R., 1998, *The Astrophysical Journal*, 497, L17
- Saxton R. D., Read A. M., Komossa S., Lira P., Alexander K. D., Wieringa M. H., 2017, *Astronomy and Astrophysics*, 598, A29
- Sironi L., Spitkovsky A., Arons J., 2013, *The Astrophysical Journal*, 771, 54
- Troja E., et al., 2017, *Nature*, 551, 71
- Troja E., et al., 2020, *Monthly Notices of the Royal Astronomical Society*, 498, 5643
- Troja E., et al., 2022, *Monthly Notices of the Royal Astronomical Society*, 510, 1902
- Waxman E., 1997a, *The Astrophysical Journal*, 485, L5
- Waxman E., 1997b, *The Astrophysical Journal*, 491, L19
- Waxman E., 2006, *Plasma Physics and Controlled Fusion*, 48, B137

## APPENDIX A:

This paper has been typeset from a  $\text{\TeX}/\text{\LaTeX}$  file prepared by the author.